Joint spatio-temporal analysis of a linear and a directional variable: space-time modeling of wave heights and wave directions in the Adriatic Sea

Fangpo Wang[1], Alan E. Gelfand[1] and Giovanna Jona-Lasinio[2]

[1]*Duke University and* [2]*University of Rome Sapienza*

Supplementary Material

S1 A data example for static joint models in Section 2

We study wave heights and directions in the Adriatic Sea, a semi-enclosed basin (Picone (2013)). The orography of the Adriatic Sea plays a key role in any study of associated wave behavior as most of the waves tend to travel from north-northwest in a south-easterly direction along the major axis of the basin.

The wave height data we employ in this paper are significant wave heights. The significant wave height (SWH) is essentially the average height of the highest waves in a wave group. The traditional definition of the significant wave height, denoted as H_s, is the average of the one-third highest wave heights (trough to crest) observed in the region. Recently, a more commonly used definition is four times the standard deviation of the vertical displacement of the sea surface (elevation), which is calculated on the basis of the wave spectrum. Corresponding to the latter definition, a notation H_{m0} is often used. With regard to directions, outgoing wave directions are often preferred to incoming and are recorded in degrees relative to a fixed orientation.

Monitored buoy data, supplying wave height and wave direction measurements would seem to be attractive for such analysis. However, at present, buoy networks are too sparse to be used as a data source for spatial analysis. Therefore, we employ an alternative data source for wave heights and wave directions, outputs from deterministic models, usually climatic forecasts computed at several *spatial* and *temporal* resolutions. These models are increasingly accurate and may be eventually calibrated using buoy data, a data fusion problem. However, here we illustrate solely with deterministic model output.

We employ the foregoing general modeling framework, illustrating with deterministic model output. In particular, we use data outputs from a deterministic wave model

implemented by ISPRA (Istituto Superiore per la Protezione e la Ricerca Ambientale) using the Hydro-Meteorological-Marine System ('Sistema Idro-Meteo-Mare', SIMM) (Speranza et al. (2004, 2007)). This integrated forecasting system includes a wind forecast model (BOLAM) predicting the surface wind (wind at 10 meters above the sea surface) over the entire Mediterranean and wave models (in deep and shallow waters).

The deep water WAve Model (WAM) describes the evolution of sea wave spectra by solving energy transport equations, using as input only the wind forecast produced from the BOLAM. Wave spectra are locally modified using a source function describing the wind energy, the energy redistribution due to nonlinear wave interactions, and energy dissipation due to wave fracture. The WAM produces significant wave height, mean wave directions (always computed over one hour time window), and the peak wave period. The model provides forecasts over a grid with 10×10 km cells every hour. The ISPRA dataset has forecasts on a total of 4941 grid points over the Italian Mediterranean. Over the Adriatic Sea area, we have 1494 points.

According to meteorologists, the definition of "calm" in the Adriatic Sea refers to a time period with wave height lower than 1 meter. When the wave height is between 1 and 2 meters, a pre-storm warning is triggered and above 2 meters there is a storm warning. We plot the data, wave directions and wave heights, for an illustrative hour under each sea state, in Figures S1.1(a)-(c), with arrow plots for the wave directions and image plot (color) for the wave heights. We apply the joint modeling framework proposed in Section 2.1 separately to each of the three datasets, respectively representing calm, transition and storm in the Adriatic Sea, as shown in Figures S1.1(a)-(c). In the absence of covariates, we employ the joint model in Section 2.1.

We model the heights directly. With concern about negative predictions, we also fitted our model with log wave heights. The results do not change; negative predictions are infrequent, even in the calm state. We also note that the stationarity assumption is likely unrealistic for coastal data due to anticipated orographic influences; our model specification is an initial attempt.

There are 1494 locations (grid points) in the Adriatic Sea and we randomly selected 300 (approximately 20%) locations for the purpose of validation. We note that the maximum interpoint distance over the set of locations is 850 km. For the fitting, we ran the MCMC algorithm for 25000 iterations with a burn-in of 5000 and thinning by collecting every fifth sample. The kriging estimates were computed using 4000 posterior samples.

The prior setting for $\mathbf{\Psi}_\theta$ was as follows: $\boldsymbol{\mu} \sim N(\mathbf{0}, 4\mathbf{I})$, $\tau_\theta^2 \sim IG(2,1)$ and $\rho \sim \text{Unif}(-1,1)$. A continuous uniform prior $\text{Unif}(0.0004, 0.1)$ was used for ϕ_θ, corresponding to a maximum and minimum range of 7500 km and 30 km, respectively. The strong spatial dependence for the directions under storm conditions suggest that we may require a range beyond the largest pairwise distance in the dataset when there is little variation in wave directions. For the parameters associated with the heights $\mathbf{\Psi}_h = \{\boldsymbol{\beta}, \tau_h^2, \sigma_h^2, \phi_h\}$, a continuous uniform prior $\text{Unif}(0.005, 0.5)$ was used for ϕ_h, corresponding to a maximum and minimum range of 600 km and 60 km, respectively. Since ϕ_h is the decay parameter in the regular linear spatial regression model, we can adopt customary priors for ranges

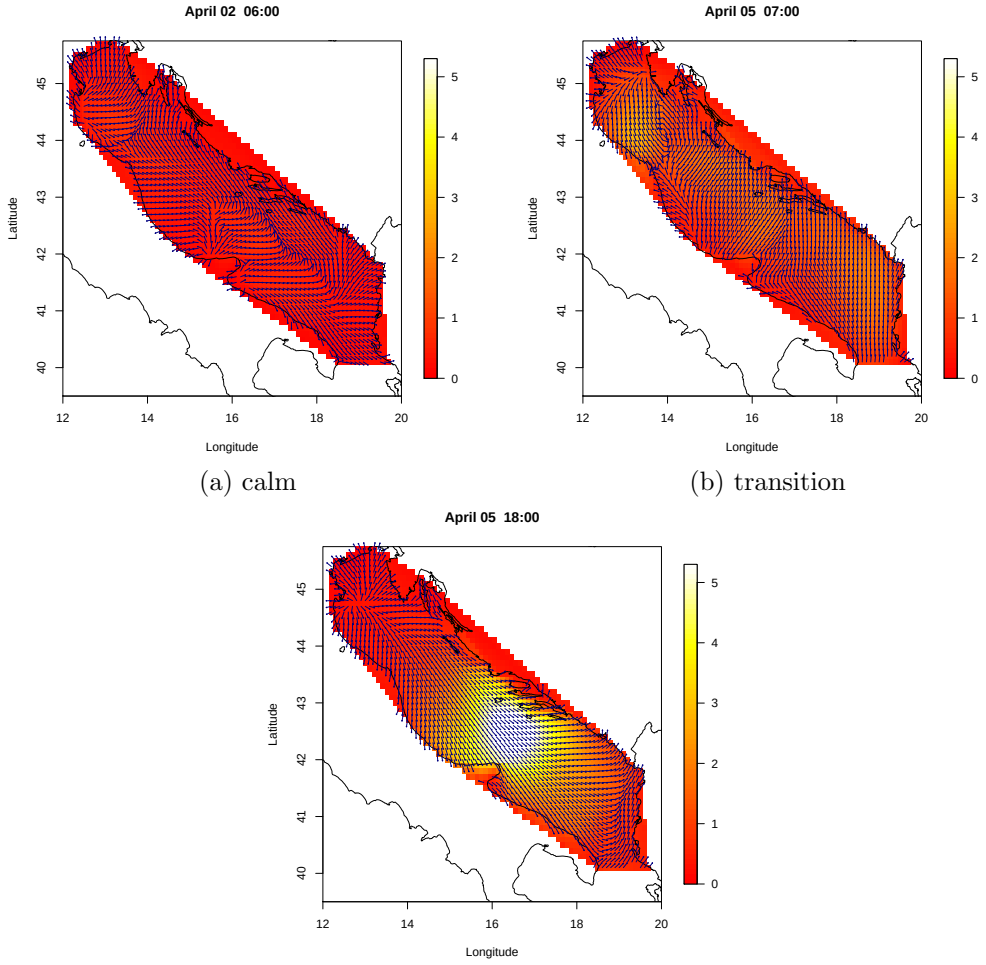

(a) calm (b) transition

(c) storm

Figure S1.1: Plot of wave heights (meters) and wave directions under three sea states: (a) calm, (b) transition and (c) storm

with linear variables. We employed a non-informative prior for $\boldsymbol{\beta}$ as $\boldsymbol{\beta} \sim N_3(\mathbf{0}, 10\mathbf{I})$. Inverse gamma priors were used for τ_h^2 and for σ_h^2, again $IG(2,1)$. These inverse gamma priors are weak in that they have infinite variance with mean 1. We did not find evidence of much sensitivity to their centering.

We compare our results with those based upon independently modeling the spatial wave height and the spatial wave direction, a nested case of our joint modeling framework obtained by setting β_1 and β_2 to be zero. In the independence case, the marginal model

for wave heights is a spatial regression with constant mean β_0, written as

$$H(\mathbf{s}) = \beta_0 + w(\mathbf{s}) + \epsilon(\mathbf{s}),\ w(\mathbf{s}) \sim GP(\mathbf{0}, \sigma_h^2 \varrho_h(\mathbf{s}-\mathbf{s}';\phi_h)),\ \epsilon(\mathbf{s}) \overset{\text{iid}}{\sim} N(0,\tau_h^2),$$

where the parameters set is $\mathbf{\Psi}_{hm} = \{\beta_0, \phi_h, \sigma_h^2, \tau_h^2\}$. The marginal model for wave directions is a constant mean projected Gaussian process model.

The posterior summaries of parameters are shown in Table S1.1, for both the joint model and the independence model above. The 95% credible intervals were obtained as approximate highest posterior density (HPD) intervals following Chen and Shao (1999). Model comparison between the joint model and the independence model is provided in Table S1.2. Regarding choice of model comparison criterion, for circular variables we utilized the continuous ranked probability score (CRPS) and the predictive log scoring loss (PLSL), following the discussion in Wang and Gelfand (2014). For the linear variables, predictive mean square error and average length of 95% credible intervals were evaluated for each model.

During a calm day, we observe small values of wave heights (lower than 1 meter) and large variation in wave directions over the region of interest. Conversely, at a time point during the storm, we observe that wave directions are fairly homogeneous while there is a large variation in wave heights over the region (ranging from 1 meter up to 6 meters). During the transition period, there is considerable variation both in wave heights and wave directions. From Table S1.1, the posterior means of the spatial variance component for wave heights under the joint model (σ_h^2) are 0.0051, 0.0344 and 0.0702 for the three datasets. Since the contribution of τ_h^2 is relatively negligible, these differences across time points agree with our remark regarding increasing variation of wave heights from calm to storm.

For the wave directions, there is no single parameter which can capture the variation across the region. Specifically, it is difficult to glean much from the posterior summaries of the parameters of the marginal projected normal distribution since the four parameters of a general projected normal altogether determine the shapes in a complex fashion. However, the decay parameter ϕ_θ associated with the spatial correlation kernel of the projected Gaussian process provide some indication of the smoothness of the surface of directions. For the calm day, ϕ_θ is much larger than in the other two cases, indicating less smoothness in this surface, as expected.

With prediction as an objective, we can consider the predictive densities of wave height and wave direction at kriged locations. For illustration, the results for one selected location at the three different sea states are shown in Figure S1.2. During the calm period, the joint model does not show much improvement in predictions in terms of concentration of the predictive densities. During the transition period, the difference between the joint model and independent models becomes a bit more clear; both of the predictive densities in Figure S1.2(b) show that the joint model outperforms the independent one. Finally, in Figure S1.2(c), we see considerable benefit to the joint model.

Turning to the model comparison results in Table S1.2, during the calm days, the model comparison criteria find the performance of the two models to be essentially

Table S1.1: Posterior summaries of the parameters: the joint model (H, Θ) and independent models H, Θ

parameter	mean	lower	upper	mean	lower	upper
data (Calm)		(H, Θ)			H, Θ	
β_0	0.2446	0.1965	0.2950	0.2331	0.1859	0.2809
β_1	0.0125	-0.0209	0.0471	-	-	-
β_2	0.0653	0.0501	0.0796	-	-	-
σ_h^2	0.0051	0.0046	0.0056	0.0055	0.0051	0.0060
τ_h^2	0.0011	0.0010	0.0013	0.0011	0.0010	0.0013
ϕ_h	0.0101	0.0084	0.0126	0.0126	0.0105	0.0116
ϕ_θ	0.0020	0.0019	0.0022	0.0019	0.0017	0.0022
μ_1	0.2856	-0.4046	0.9755	0.3039	-0.4310	1.0000
μ_2	-0.5055	-1.7615	0.8260	-0.4141	-1.6671	0.9952
τ_θ^2	0.2717	0.2275	0.3137	0.2747	0.2388	0.3180
ρ	-0.4874	-0.5713	-0.4268	-0.4790	-0.5451	-0.4078
data (Transition)		(H, Θ)			H, Θ	
β_0	0.4660	0.3244	0.6176	0.5394	0.3685	0.6892
β_1	0.1887	0.1281	0.2453	-	-	-
β_2	0.3062	0.2478	0.3706	-	-	-
σ_h^2	0.0344	0.0306	0.0389	0.0413	0.0376	0.0482
τ_h^2	0.0021	0.0019	0.0024	0.0021	0.0018	0.0023
ϕ_h	0.0101	0.0084	0.0126	0.0084	0.0072	0.0090
ϕ_θ	0.0006	0.0005	0.0007	0.0006	0.0005	0.0007
μ_1	-0.1066	-2.3975	2.1270	0.0617	-2.0922	2.2151
μ_2	-0.2935	-1.7928	1.3506	-0.2152	-1.8580	1.3850
τ_θ^2	2.4400	2.0958	2.8055	2.2318	1.9602	2.5818
ρ	-0.2264	-0.3069	-0.1473	-0.2257	-0.2994	-0.1430
data (Storm)		(H, Θ)			H, Θ	
β_0	0.3795	0.1897	0.5776	0.4737	0.0734	0.8790
β_1	-0.3052	-0.4049	-0.2066	-	-	-
β_2	0.8794	0.7588	0.9883	-	-	-
σ_h^2	0.0702	0.0546	0.0826	0.1930	0.1677	0.2283
τ_h^2	0.0033	0.0028	0.0038	0.0034	0.0028	0.0039
ϕ_h	0.0105	0.0087	0.0122	0.0070	0.0063	0.0076
ϕ_θ	0.0006	0.0005	0.0007	0.0006	0.0005	0.0007
μ_1	0.5853	-0.8418	1.8745	0.6990	-0.5824	2.0369
μ_2	-0.6064	-2.0949	0.9097	-0.5152	-2.0546	0.9437
τ_θ^2	0.7216	0.6515	0.7917	0.7312	0.6652	0.8070
ρ	-0.6433	-0.6827	-0.6018	-0.6631	-0.7107	-0.6105

Table S1.2: Model comparison: the joint model (H, Θ) and independent models H, Θ

	(a) calm		(b) transition		(c) storm	
Feature	(H, Θ)	H, Θ	(H, Θ)	H, Θ	(H, Θ)	H, Θ
Predictive Mean Square Error (height)	0.0006	0.0006	0.0031	0.0030	0.0109	0.0108
Average Length of 95% Credible Interval (height)	0.1821	0.1788	0.3405	0.3586	0.5163	0.6345
mean CRPS for wave direction	0.0407	0.0408	0.0276	0.0279	0.0213	0.0223
PLSL for wave direction	-977	-974	-1098	-1104	-1321	-1318

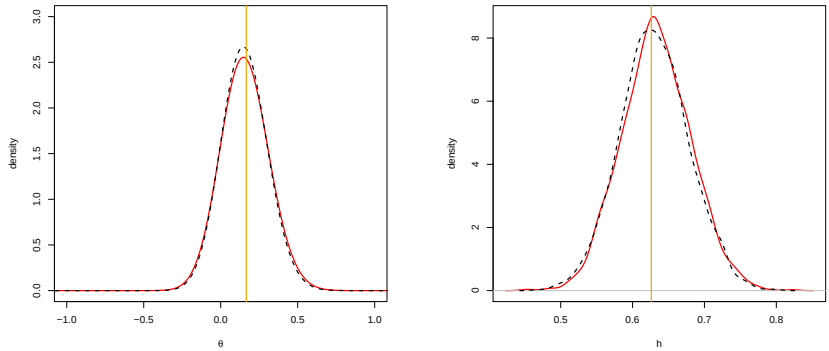

(a) calm

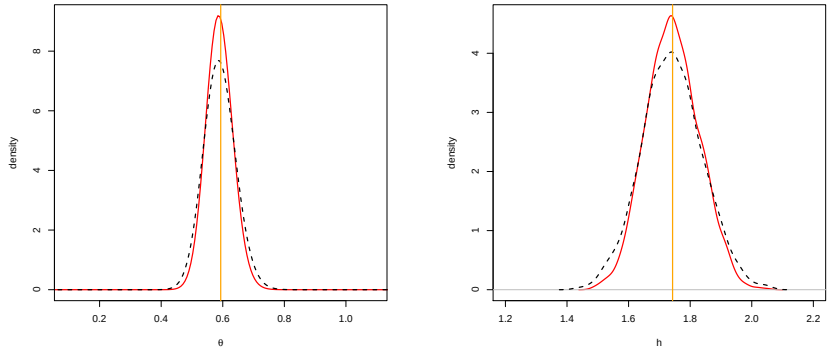

(b) transition

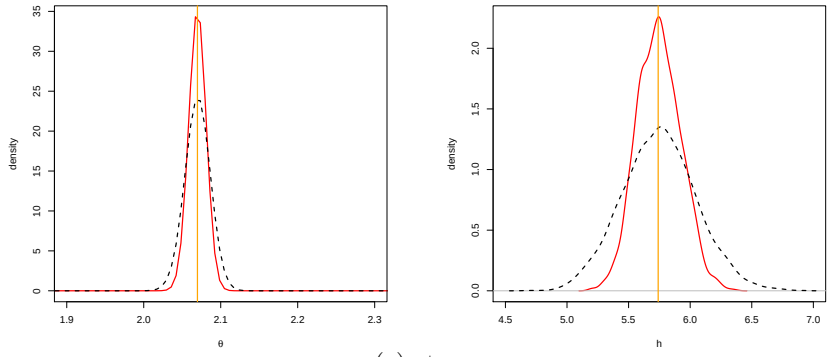

(c) storm

Figure S1.2: Predictive densities of directions (left) and heights (right) at one kriged location during different sea states: the solid line is for the joint model (H, Θ), the dashed line is for the independent model H, Θ, and the vertical line shows the held-out observation

equivalent. For the transition case, the joint model emerges as slightly better, with shorter average length of 95% credible intervals and slightly smaller average CPRS and PLSL. For the time point chosen during a storm, the biggest gain is achieved. We have a substantially narrower average length of credible intervals and a roughly 5% smaller value of CRPS. Such model comparison results are supported by the predictive density examination in Figure S1.2.

As mentioned previously, the independence model is nested in the joint model framework. The posterior summaries of β_1 and β_2 in Table S1.1 concur with these findings. For the time point during a calm day, β_1 and β_2 are nearly zero, which supports the independence of wave heights and wave directions. As we move from calm to transition to storm, the β_1 and β_2 become increasingly different from 0. The multiple correlation coefficient is computed, as in (2.5), and we show the posterior densities of the multiple correlation coefficient for all three scenarios in Figure S1.3. The figure concisely supports Table S1.1, revealing stronger association between height and direction as we move from calm to storm. Finally, we note that the negative β_1 and positive β_2 are not unexpected. With storms tending to travel from the north-northwest to the southeast, and with the *sin* increasing and *cos* decreasing in these directions, this supplies an expectation of an increase in wave height as a function of θ as the storm develops.

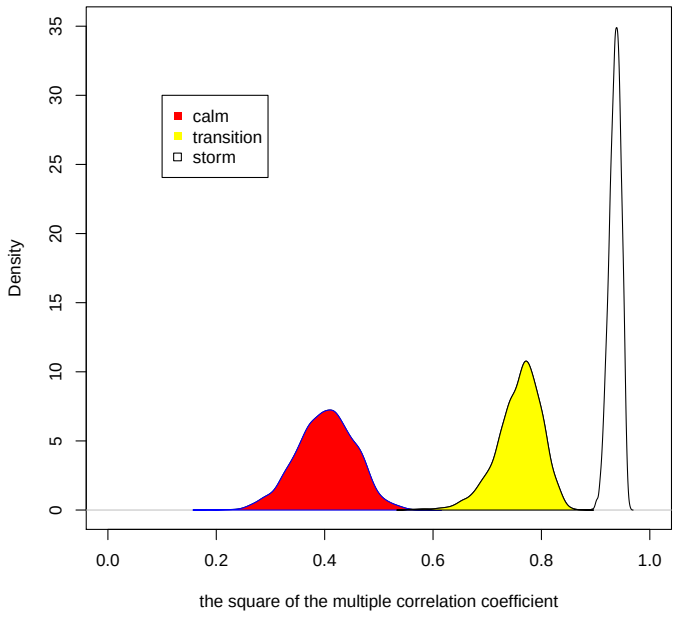

Figure S1.3: The posterior densities of the square of the multiple correlation coefficient $R^2_{H|\mathbf{Y}}$

Table S2.1: Posterior summaries of the parameters (mean and HPD)

	(calm)			(storm)		
parameter	mean	lower	upper	mean	lower	upper
β_0	0.1612	0.0563	0.2998	0.5483	-0.0218	1.1750
β_1	-0.0117	-0.0388	0.0161	-0.1439	-0.2805	-0.0171
β_2	0.0329	0.0112	0.0563	0.2061	0.0650	0.3529
σ_h^2	0.3561	0.2916	0.4315	8.2797	6.8463	10.0983
τ_h^2	0.0020	0.0017	0.0024	0.0091	0.0064	0.0119
ϕ_h	0.0051	0.0048	0.0056	0.0047	0.0043	0.0051
μ_1	0.2999	-0.2808	0.8955	0.1835	-0.6192	0.9448
μ_2	-0.1431	-0.9733	0.6035	-0.0868	-0.9079	0.6537
τ^2	0.6129	0.5665	0.6448	0.9245	0.8879	0.9972
ρ	-0.7095	-0.7359	-0.6878	-0.6251	-0.6656	-0.5905
$\phi_{\theta,\mathbf{s}}$	0.0043	0.0037	0.0050	0.0022	0.0020	0.0024
$\phi_{\theta,t}$	0.0775	0.0750	0.0803	0.1667	0.1487	0.1782

S2 A data example for joint space-time models in Section 3

For illustration, we randomly selected a small fraction of the locations ($n = 200$) from the same data set in Section S1 of the online Supplement. These locations are those in both Figure 1 and Figure 2. Recalling the definition of calm and storm in Section S1, Figure 2 also provides information regarding the time intervals of calm and storm. Our goal here is to illustrate the prediction at a future time point t_{k+1} within each interval, using our joint space-time model.

We selected data from a calm period, April 2nd to April 3rd, 2010. The time points are collected every two hours. Thus starting from April 2nd, 00:00 to April 3rd 22:00, we have 24 time points in total. In addition, we selected data from a severe storm period, April 5th to April 6th. Again, the time points are collected at the same temporal resolution, every two hours. Thus starting from April 5th, 00:00 to April 6th 22:00, with 24 time points in total. In both cases, we held out the observation at the last time point for forecasting validation.

The posterior summaries of the regression coefficients for the conditional specification are reported in Table S2.1. During the calm period, β_1 and β_2 are nearly zero, agreeing with the results for a single time slice during the calm period shown in Section S1. This suggests that approximate independence of wave heights and wave directions sustains during a calm period. However, during a storm period, β_1 and β_2 clearly depart from zero, indicating strong dependence of wave heights and wave directions during the storm, again consistent with the results in Section S1. We see that, again, σ_h^2 dominates the variation in heights and we see more than a twenty-fold increase during the storm period. With regard to the decay parameters, $\phi_{\theta,\mathbf{s}}$ is roughly double in calm compared with storm (the spatial range is roughly half), while $\phi_{\theta,t}$ is roughly half in calm compared with storm (the temporal range is roughly double).

We are interested in the result of prediction at the future time point t_{k+1}. Table

Table S2.2: Summaries for one-step ahead prediction

	calm	storm
Predictive Mean Square Error (height)	0.0522	0.4497
mean CRPS for wave direction	0.0973	0.0647

S2.2 provides the summaries of prediction for both wave heights and wave directions. We do not use any information at time t_{k+1} to fit the model; however, the model provides reasonable prediction. We predict direction better in a storm (expected since there is less variability in direction during a storm) and height dramatically better during a calm period (again, expected because heights are lower and less variable when it is calm), in agreement with the results from Table S2.1.

We have also looked at a dynamic model specification. The implicit challenge lies in the transition specification, the marginal distributions of the directions under the projected normal have shapes that depend jointly, in a complex way, on all four parameters in $\boldsymbol{\mu}$ and T. One would need to introduce a four dimensional joint dynamic specification for them; dynamics in just say, $\boldsymbol{\mu}$ are not enough. Then, one must address dynamics in the parameters for the conditional specification for heights given directions. Altogether, we found such second stage vector autoregressive models very difficult to specify, even more difficult to fit, especially with shorter time series. Moreover, if these parameters are only indexed by time, then we will still have space-time separability.

S3 Appendix A: Mean and cross-covariance structures of $(H(\mathbf{s}), Y_1(\mathbf{s}), Y_2(\mathbf{s}))^{\mathrm{T}}$

In Section 2.1, $(H(\mathbf{s}), Y_1(\mathbf{s}), Y_2(\mathbf{s}))^{\mathrm{T}}$ follows a trivariate Gaussian process. The mean structure of this Gaussian process is $(\beta_0+\beta_1\mu_1+\beta_2\mu_2, \mu_1, \mu_2)^{\mathrm{T}}$ and the cross-covariance is

$$C_{H,\mathbf{Y}}(\mathbf{s},\mathbf{s}') = \varrho_\theta(\mathbf{s}-\mathbf{s}';\phi_\theta)\begin{pmatrix} v_{11} & v_{12} & v_{13} \\ v_{21} & & \\ v_{31} & & \end{pmatrix} + \varrho_h(\mathbf{s}-\mathbf{s}';\phi_h)\begin{pmatrix} \sigma_h^2+\tau_h^2\mathbf{1}_{\mathbf{s}=\mathbf{s}'} & \mathbf{0}_{1\times 2} \\ \mathbf{0}_{2\times 1} & \mathbf{0}_{2\times 2} \end{pmatrix},$$

where $v_{11} = \beta_1^2\tau_\theta^2 + 2\beta_1\beta_2\rho\tau_\theta + \beta_2^2$, $v_{12} = v_{21} = \beta_1\tau_\theta^2 + \beta_2\rho\tau_\theta$, $v_{13} = v_{31} = \beta_1\rho\tau_\theta + \beta_2$ and $T = \begin{pmatrix} \tau_\theta^2 & \rho\tau_\theta \\ \rho\tau_\theta & 1 \end{pmatrix}$.

S4 Appendix B: Posterior Computation: The full conditionals of Ψ_h and Ψ_θ

In Section 2.2, $\mathbf{\Psi}_h = \{\boldsymbol{\beta}, \phi_h, \sigma_h^2, \tau_h^2\}$ and $\mathbf{\Psi}_\theta = \{\boldsymbol{\mu}, T, \phi_\theta\}$, where $T = \begin{pmatrix} \tau_\theta^2 & \rho\tau_\theta \\ \rho\tau_\theta & 1 \end{pmatrix}$.

We define two covariance matrices $\tilde{\Sigma}_\theta = T \otimes \mathbf{\Gamma}_\theta(\phi_\theta)$ and $\tilde{\Sigma}_\theta^* = \mathbf{\Gamma}_\theta(\phi_\theta) \otimes T$. Their corresponding precision matrices are $\tilde{Q}_\theta = \tilde{\Sigma}_\theta^{-1} = T^{-1} \otimes \mathbf{\Gamma}_\theta^{-1}(\phi_\theta)$ and $\tilde{Q}_\theta^* = \tilde{\Sigma^*}_\theta^{-1} = \mathbf{\Gamma}_\theta^{-1}(\phi_\theta) \otimes T^{-1}$. $\Gamma_{\theta,ij}^{-1}$ denotes the element on the i-th row and j-th column of the inverse matrix of $\mathbf{\Gamma}_\theta(\phi_\theta)$.

Following (2.3), the top or conditional hierarchy can be written as,

$$\begin{aligned} H(\mathbf{s}) &= \beta_0 + R(\mathbf{s})[\beta_1 \cos\Theta(\mathbf{s}) + \beta_2 \sin\Theta(\mathbf{s})] + w(\mathbf{s}) + \epsilon(\mathbf{s}), \\ &= \beta_0 + R(\mathbf{s})\beta_4(\mathbf{s}) + w(\mathbf{s}) + \epsilon(\mathbf{s}). \end{aligned}$$

As defined in Section 2.2, $\Sigma_h = \sigma_h^2 \mathbf{\Gamma}(\phi_h) + \tau_h^2 I_n$. The inverse matrix of Σ_h is denoted as Q_h, with $Q_{h,ij}$ representing its element on the i-th row and j-th column. We then write $\tilde{H}(\mathbf{s}) = H(\mathbf{s}) - \beta_0$, so $\tilde{H}(\mathbf{s}) = R(\mathbf{s})\beta_4(\mathbf{s}) + w(\mathbf{s}) + \epsilon(\mathbf{s})$. The conditional distribution of $\tilde{H}(\mathbf{s}_i)$ given $\tilde{H}(-\mathbf{s}_i)$ can be easily obtained as a normal distribution, with $R(\mathbf{s}_i)$ involved in the mean.

The full conditionals for the parameters of the joint process model:

- $\boldsymbol{\mu} \sim \mathrm{N}_2(E_\mu, Q_\mu^{-1})$, where the precision matrix of this bivariate normal $Q_\mu = A^{\mathrm{T}}\tilde{\Sigma}_\theta^{-1}A + I_2/\lambda_\mu$, $E_\mu = Q_\mu^{-1}A^{\mathrm{T}}\tilde{\Sigma}_\theta^{-1}\mathbf{Y}$,and $A = \begin{pmatrix} \mathbf{1}_{n\times 1} & \mathbf{0}_{n\times 1} \\ \mathbf{0}_{n\times 1} & \mathbf{1}_{n\times 1} \end{pmatrix}$.
- $$\begin{aligned} &R(\mathbf{s}_i) \propto r_i I_{(0,\infty)}(r_i) \\ &\qquad \exp\left(-\frac{(\Gamma_{\theta,ii}^{-1}\mathbf{u}_i^{\mathrm{T}}T^{-1}\mathbf{u}_i + \beta_4^2(\mathbf{s}_i))r_i^2 - 2r_i(\Gamma_{\theta,ii}^{-1}\mathbf{u}_i^{\mathrm{T}}T^{-1}E_{si} + \beta_4(\mathbf{s}_i)E_{si2})}{2}\right), \end{aligned}$$

  where $\mathbf{u}_i = (\cos\theta(\mathbf{s}_i), \sin\theta(\mathbf{s}_i))^{\mathrm{T}}$, $E_{si} = \boldsymbol{\mu} - Q_{si}^{-1}\sum_{j\neq i}\tilde{Q}_{\theta,ij}^*(\mathbf{Y}(\mathbf{s}_j) - \boldsymbol{\mu})$,$Q_{si} = \tilde{Q}_{\theta,ii}^* = \Gamma_{\theta,ii}^{-1}\cdot T^{-1}$, $E_{si2} = \tilde{h}(\mathbf{s}_i) + Q_{h,ii}^{-1}\sum_{j\neq i}Q_{h,ij}[\tilde{h}(\mathbf{s}_j) - r_j\beta_4(\mathbf{s}_j)]$,and $\tilde{Q}_{\theta,ij}^* = \Gamma_{\theta,ij}^{-1}\cdot T^{-1}$.
- $\phi_\theta \propto |\mathbf{\Gamma}_\theta(\phi_\theta)|^{-1}\exp\left(-(\mathbf{Y} - A\boldsymbol{\mu})^{\mathrm{T}}T^{-1} \otimes \mathbf{\Gamma}_\theta^{-1}(\phi_\theta)(\mathbf{Y} - A\boldsymbol{\mu})/2\right)$.
- $$\begin{aligned} &\tau_\theta^2, \rho \propto |T|^{-n/2}\exp\left(-(\mathbf{Y} - A\boldsymbol{\mu})^{\mathrm{T}}T^{-1} \otimes \mathbf{\Gamma}_\theta^{-1}(\phi_\theta)(\mathbf{Y} - A\boldsymbol{\mu})/2\right) \\ &\qquad (\tau_\theta^2)^{-a_{\tau\theta}-1}\exp(-b_{\tau\theta}/\tau_\theta^2). \end{aligned}$$

- $\boldsymbol{\beta} \sim \mathrm{N}_3(E_\beta, Q_\beta^{-1})$, where the precision matrix of the multivariate normal $Q_\beta = \mathbf{X}^\mathrm{T}\Sigma_h^{-1}\mathbf{X}$, $E_\beta = Q_\beta^{-1}\mathbf{X}^\mathrm{T}\Sigma_h^{-1}\mathbf{h}$, $\mathbf{h} = (h(\mathbf{s}_1), \ldots, h(\mathbf{s}_n))^\mathrm{T}$, $\mathbf{X}$ is a $n \times 3$ matrix with the i-th row as $(1, r(\mathbf{s}_i)\cos\theta(\mathbf{s}_i), r(\mathbf{s}_i)\sin\theta(\mathbf{s}_i))$, $i = 1, \ldots, n$.
- $\phi_h \propto |\Sigma_h|^{-1/2}\exp\left(-\frac{(\mathbf{h}-\mathbf{X}\boldsymbol{\beta})^\mathrm{T}\Sigma_h^{-1}(\mathbf{h}-\mathbf{X}\boldsymbol{\beta})}{2}\right)$, where $\Sigma_h = \tau_h^2\boldsymbol{\Gamma}_h^{-1}(\phi_h) + \sigma_h^2 I_n$.
- $$\tau_h^2, \sigma_h^2 \propto |\Sigma_h|^{-1/2}\exp\left(-\frac{(\mathbf{h}-\mathbf{X}\boldsymbol{\beta})^\mathrm{T}\Sigma_h^{-1}(\mathbf{h}-\mathbf{X}\boldsymbol{\beta})}{2}\right)(\tau_h^2)^{-a_{\tau h}-1} \exp(-b_{\tau h}/\tau_h^2)(\sigma_h^2)^{-a_{\sigma h}-1}\exp(-b_{\sigma h}/\tau_h^2).$$

References

Chen, M.-H. and Shao, Q.-M. (1999). Monte Carlo estimation of Bayesian credible and HPD intervals. *J. Comput. Graph. Stat.* **8**, 69-92.

Picone, M. (2013). Model Based Clustering of Mixed Linear and Circular Data. Ph.D. thesis. Roma Tre University.

Speranza, A., Accadia, C., Casaioli, M., Mariani, S., Monacelli, G., Inghilesi, R., Tartaglione, N., Ruti, P. M., Carillo, A., Bargagli, A., Pisacane, G., Valentinotti, F., and Lavagnini, A. (2004). POSEIDON: An integrated system for analysis and forecast of hydrological, meteorological and surface marine fields in the Mediterranean area. *Nuovo Cimento C* **27**, 329-345.

Speranza, A., Accadia, C., Mariani, S., Casaioli, M., Tartaglione, N., G. Monacelli, P. M. R., and Lavagnini, A. (2007). SIMM: An integrated forecasting system for the Mediterranean area. *Meteorol. Appl.* **14**, 337-350.

Wang, F. and Gelfand, A. E. (2014). Modeling space and space-time directional data using projected Gaussian processes. *Journal of the American Statistical Association* **109**, doi:10.1080/01621459.2014.934454.